Title

Technique for real-time tissue characterization based on scanning multispectral fluorescence lifetime spectroscopy (ms-TRFS)

Journal

Biomedical Optics Express, 6(3)

ISSN

2156-7085

Authors

Ma, Dinglong
Bec, Julien
Gorpas, Dimitris
et al.

Publication Date

2015-03-01

DOI

10.1364/boe.6.000987

Peer reviewed

Biomedical Optics EXPRESS

Technique for real-time tissue characterization based on scanning multispectral fluorescence lifetime spectroscopy (ms-TRFS)

Dinglong Ma,[1] Julien Bec,[1] Dimitris Gorpas,[1] Diego Yankelevich,[1,2] and Laura Marcu[1,*]

[1]*Department of Biomedical Engineering, University of California, Davis, 451 Health Science Dr., Davis, CA 95616 USA*

[2]*Department of Electrical and Computer Engineering, University of California, Davis, One Shields Ave., Davis, CA 95616 USA*

[*]*lmarcu@ucdavis.edu*

Abstract: We report a novel technique for continuous acquisition, processing and display of fluorescence lifetimes enabling real-time tissue diagnosis through a single hand held or biopsy fiber-optic probe. A scanning multispectral time-resolved fluorescence spectroscopy (ms-TRFS) with self-adjustable photon detection range was developed to account for the dynamic changes of fluorescence intensity typically encountered in clinical application. A fast algorithm was implemented in the ms-TRFS software platform, providing up to 15 Hz continuous display of fluorescence lifetime values. Potential applications of this technique, including biopsy guidance, and surgical margins delineation were demonstrated in proof-of-concept experiments. Current results showed accurate display of fluorescence lifetimes values and discrimination of distinct fluorescence markers and tissue types in real-time (< 100 ms per data point).

OCIS codes: (300.6500) Spectroscopy, time-resolved; (170.6510) Spectroscopy, tissue diagnostics; (170.6935) Tissue characterization.

References and links

1. D. Savastru, E. W. Chang, S. Miclos, M. B. Pitman, A. Patel, and N. Iftimia, "Detection of breast surgical margins with optical coherence tomography imaging: a concept evaluation study," J. Biomed. Opt. **19**(5), 056001 (2014).
2. A. C. Croce, A. Ferrigno, G. Santin, V. M. Piccolini, G. Bottiroli, and M. Vairetti, "Autofluorescence of Liver Tissue and Bile: Organ Functionality Monitoring During Ischemia and Reoxygenation," Lasers Surg. Med. **46**(5), 412–421 (2014).
3. C. Kallaway, L. M. Almond, H. Barr, J. Wood, J. Hutchings, C. Kendall, and N. Stone, "Advances in the clinical application of Raman spectroscopy for cancer diagnostics," Photodiagn. Photodyn. Ther. **10**(3), 207–219 (2013).
4. L. Marcu, "Fluorescence Lifetime Techniques in Medical Applications," Ann. Biomed. Eng. **40**(2), 304–331 (2012).
5. Y. Sun, R. Liu, D. S. Elson, C. W. Hollars, J. A. Jo, J. Park, Y. Sun, and L. Marcu, "Simultaneous time- and wavelength-resolved fluorescence spectroscopy for near real-time tissue diagnosis," Opt. Lett. **33**(6), 630–632 (2008).
6. Y. H. Sun, Y. Sun, D. Stephens, H. T. Xie, J. Phipps, R. Saroufeem, J. Southard, D. S. Elson, and L. Marcu, "Dynamic tissue analysis using time- and wavelength-resolved fluorescence spectroscopy for atherosclerosis diagnosis," Opt. Express **19**(5), 3890–3901 (2011).
7. J. Bec, D. M. Ma, D. R. Yankelevich, J. Liu, W. T. Ferrier, J. Southard, and L. Marcu, "Multispectral fluorescence lifetime imaging system for intravascular diagnostics with ultrasound guidance: in vivo validation in swine arteries," J. Biophotonics **7**, 281–285 (2013).
8. H. Fatakdawala, S. Poti, F. Zhou, Y. Sun, J. Bec, J. Liu, D. R. Yankelevich, S. P. Tinling, R. F. Gandour-Edwards, D. G. Farwell, and L. Marcu, "Multimodal in vivo imaging of oral cancer using fluorescence lifetime, photoacoustic and ultrasound techniques," Biomed. Opt. Express **4**(9), 1724–1741 (2013).
9. H. T. Xie, J. Bec, J. Liu, Y. Sun, M. Lam, D. R. Yankelevich, and L. Marcu, "Multispectral scanning time-resolved fluorescence spectroscopy (TRFS) technique for intravascular diagnosis," Biomed. Opt. Express **3**(7), 1521–1533 (2012).

#228925 - $15.00 USD Received 10 Dec 2014; revised 19 Feb 2015; accepted 20 Feb 2015; published 25 Feb 2015

10. D. R. Yankelevich, D. Ma, J. Liu, Y. Sun, Y. Sun, J. Bec, D. S. Elson, and L. Marcu, "Design and evaluation of a device for fast multispectral time-resolved fluorescence spectroscopy and imaging," Rev. Sci. Instrum. **85**(3), 034303 (2014).
11. A. Isidori, L. Marconi, and A. Serrani, "Fundamentals of Internal-Model-Based Control Theory," in *Robust Autonomous Guidance* (Springer London, 2003), pp. 1–58.
12. J. Liu, Y. Sun, J. Y. Qi, and L. Marcu, "A novel method for fast and robust estimation of fluorescence decay dynamics using constrained least-squares deconvolution with Laguerre expansion," Phys. Med. Biol. **57**(4), 843–865 (2012).
13. C. L. H. Lawson and J. Richard, "Linear Least Squares with Linear Inequality Constraints," in *Solving Least Squares Problems*, R. E. O'Malley, Jr., ed. (1974), pp. 158–173.
14. G. Bradski, "{The OpenCV Library}," Dr. Dobb's Journal of Software Tools (2000).
15. O. Assayag, M. Antoine, B. Sigal-Zafrani, M. Riben, F. Harms, A. Burcheri, K. Grieve, E. Dalimier, B. Le Conte de Poly, and C. Boccara, "Large Field, High Resolution Full-Field Optical Coherence Tomography: A Pre-clinical Study of Human Breast Tissue and Cancer Assessment," Technol. Cancer Res. Treat. **13**(5), 455–468 (2014).
16. A. N. S. Institute, "American National Standard for Safe Use of Lasers in Health Care ANSI Z136.1," (Laser Institute of America, Orlando, FL, 2007).
17. F. del Monte, J. D. Mackenzie, and D. Levy, "Rhodamine fluorescent dimers adsorbed on the porous surface of silica gels," Langmuir **16**(19), 7377–7382 (2000).

1. Introduction

New diagnostic tools are needed to facilitate real-time (live) intra-operative diagnosis, guidance to surgery or other interventions. Optical techniques have demonstrated great potential for providing rapidly and non-invasively information about tissue anatomic [1], functional [2] and molecular [3] features. As reported by numerous research groups, fluorescence spectroscopy and imaging methods, in particular, have shown potential for tissue characterization and diagnosis with applications in numerous clinical areas including oncology, cardiology, and ophthalmology [4]. Time-resolve fluorescence measurements, in particular, were found very promising as they are less sensitive to presence of endogenous absorbers (e.g. blood) or changes in light excitation-collection geometries [4]. Moreover, a recently reported multi-spectral time-resolved fluorescence spectroscopy (ms-TRFS) technique [5] demonstrated potential for rapid acquisition of time-resolved fluorescence signal in multiple wavelength bands simultaneously with high photon throughput. Importantly, such implementation allows for continuous scanning of tissue samples both in-vitro [6] and in-vivo [7] and recording of TRFS data from large surface areas from either planar [8] or tubular structures [9]. However, in these earlier applications, the TRFS data were first recorded from the entire area of interest, then analyzed to determine the actual fluorescence decay characteristics (e.g. fluorescence lifetime(s)), and finally the results carrying diagnostic information were displayed. Typically such process requires a minimum of several seconds to a few minutes or off-line processing depending on the total number of data points and the method used for fluorescence decay analysis. While such approach represents a first step to implementation of a fast near-real-time tissue diagnostic tool it poses a few critical challenges.

First, the optical data from each measurement point or "pixel" needs to be co-registered with the location from where the measurement was actually taken. Such co-registration is difficult to achieve when the measurements are taken continuously in dynamic conditions such those encountered during *in vivo* studies where the location of the measurement may shift from the time of data recording to the time of data display. Second, a robust means for fluorescence data acquisition is required to account for sudden variation of the intensity of auto-fluorescence signal so that the variation of fluorescence photon number has minimal impact on the time-resolved fluorescence detection. Such variation is due to a number of conditions including dynamic changes of fluorescence excitation-collection geometry, the broad range of quantum efficiencies exhibited by endogenous fluorescent molecules, non-uniform illumination due to uneven tissue surface profile, and the presence/absence of strong endogenous absorbers (e.g. blood). These conditions are difficult to account for, in particular, when non-contact scanning fiber-optics probes are used and/or scanning of a large tissue

#228925 - $15.00 USD Received 10 Dec 2014; revised 19 Feb 2015; accepted 20 Feb 2015; published 25 Feb 2015

surface area is needed. Third, the analysis of fluorescence decay data needs to be integrated in the data acquisition software platform in a manner that allows for near-instantaneously display of diagnostic data during tissue scanning.

Current study aims to addressing these challenges. We report the development and evaluation of a tissue characterization technique based on a single fiber-optic ms-TRFS system with self-adjustable photon detection range. This system can robustly acquire fluorescence decay data during dynamic variation of fluorescence intensity and continuously process and display fluorescence lifetime information in real-time (<100 ms) during data acquisition. The performance of this technique was evaluated using fluorescence standards. Potential applications as a scanning-diagnostic (through mechanical or hand held movement) tool were demonstrated through proof-of-concept experiments in tissue phantoms and *in situ* brain tissue.

2. Materials and methods

2.1 ms-TRFS system specification

To implement the real-time ms-TRFS technique we employed an instrumental setup based on a pulse sampling detection method previously reported by our group [10]. The fluorescence excitation and collection was realized via single fiber-optic probes that can be configured for specific applications as described below. In brief, the fluorescence is induced using a fiber laser (Fianium HE, 355 nm, 80 ps, 10 kHz – 1 MHz, 0.5 μJ). The fluorescence emission is spectrally resolved using a custom wavelength-selection module (WSM) [10] that separates the fluorescence into four wavelength channels (center wavelength/bandwidth: 390/40, 452/45, 542/50 and 629/53 nm) coupled to four optical delay lines (1, 10, 19 and 28 m lengths), generating a 45 ns delay between channels. The fluorescence photons from all 4 channels were detected using a single micro-channel plate (MCP) photo-multiplier (PMT) (R3809U-50, Hamamatsu, 45 ps FWHM), the resulting signal output is then amplified (pre-amplifier C5594, Hamamatsu, 36 dB) and digitized (digitizer PXIe-5185, National Instrument, 12.5 GS/s sampling rate, 3 GHz analog bandwidth, 50 mV – 1V dynamic range). An embedded controller (PXIe-8102, National Instrument) was integrated with the digitizer for readout, processing and storage of the ms-TRFS data. A programmable high voltage (HV) power supply (PS350, Stanford Research Systems) provided high voltage bias to the MCP-PMT and linked with the embedded controller.

For general applications that interrogate the tissue surface, a hand held fiber-optic probe was constructed using a 400 μm core diameter, 0.22 NA silica fibers (FVP400440480, Polymicro, USA) introduced in 21 G stainless hypodermic tubing integrated with a polymer hand piece. The fiber-optic was polished at 90 degree angle to allow front-view excitation-collection. This probe can be used in line scanning and raster scanning configurations with motorized motion or manual movement. For needle biopsy application that requires fiber-optic to advance into depth of tissue, a fiber-optic probe was constructed using the same type of silica fiber and tubing while both the fiber and the tubing was cut and polished at 45 degree angle.

2.2 Closed-loop control of fluorescence detection: design and evaluation

As noted above the number of fluorescence photons reaching the detector can change dramatically during in-vivo tissue interrogation. However, a key advantage of fluorescence lifetime measurements is that they are not affected by changes in fluorescence intensity provided that a sufficient number of photons are collected to reconstruct the fluorescence decay dynamics. Typically, the high number of excitation photons ($\sim 1 \times 10^{11}$) provided by the fiber laser with more than 10 nJ delivered to tissue, combined with a relatively high quantum yield of endogenous tissue fluorophores result in sufficient fluorescence photons (10^4–10^7) to accurately recover tissue fluorescence decay. However, for a pulse sampling detection

#228925 - $15.00 USD Received 10 Dec 2014; revised 19 Feb 2015; accepted 20 Feb 2015; published 25 Feb 2015

method, a practical challenge still remains – i.e. the large range of fluorescence intensity variation cannot be covered by the small dynamic range of the high-speed digitizers (i.e. 8 – 10 bit sampling depth with approximately ± 1% full-scale accuracy). Thus, to optimize the signal amplitude (calculated as the maximum voltage corresponding to an averaged fluorescence pulse transient (waveform)) matching the digitizer dynamic range, we designed and implemented a closed-loop control algorithm (Fig. 1(a)) that provides feedback to the HV power supply which determines the gain of photon multiplication and alters the signal amplitude.

The goal of this control algorithm is to maintain the signal amplitude (V) at target signal amplitude (V_t), which is decided based on system performance evaluation described later. For this, we designed and included in the control algorithm an internal model controller (IMC) to account for the changes in steady-state intensity and a proportional controller to account for transient intensity variations. An IMC is defined here as a mechanism that simulates the response of the system in order to estimate the outcome of an input command [11]. In current study, the IMC was based on the correlation of the signal amplitude and the MCP-PMT HV bias. For a given number of fluorescence photons, the signal amplitude is determined by the variable MCP-PMT HV bias and other parameters including the radiant sensitivity of the photo-cathode in the MCP-PMT, the gain of the pre-amplifier. These other parameters were treated as constants for each channel of the ms-TRFS system. To determine the optimal MCP-PMT HV bias, the correlation between signal amplitude and the MCP-PMT HV bias was characterized experimentally. The short pulses of 532 nm second harmonic component of the fiber laser were sent into the WSM of the ms-TRFS system and detected by the MCP-PMT. The optical power of the laser pulses was measured at the input of the MCP-PMT with a power meter (PM100D, Thorlabs, S120VC, 200 – 1100 nm, 50 mW) and the pulse energy was calculated based on the laser repetition rate of 10 kHz. The HV bias was varied while the waveforms of laser pulses were recorded to track the change of signal amplitude. Using this correlation, the signal amplitude for an optical pulse with a given number of photons detected by the ms-TRFS system can be estimated as a function of the MCP HV bias. This correlation was also used to calculate the number of detected fluorescence photons when the signal amplitude and HV bias were known during ms-TRFS measurements.

To account for the limited bandwidth of the HV changes during the use of the IMC, the time response of the HV power supply was characterized. The fluorescence from a laser dye, Rhodamine 6G (R6G) measured by channel 3 of ms-TRFS was used to evaluate the HV bias transient after a command is sent from the embedded controller to the HV power supply. As shown in Fig. 1(b), step-wise HV change commands were sent to the power supply with step heights of ± 20 V, ± 50 V and ± 100 V. The transient response measured through the signal amplitude presented rise times of 0.47 – 0.56 seconds and fall times of 0.32 – 0.42 seconds. This demonstrates that IMC alone is not able to adjust the HV bias fast enough for real-time response time of less than 100 ms. Since HV changes response time are relatively independent from the step sizes, performance should be improved by preemptively increasing or lowering the HV set point to deal with high speed transient changes of fluorescence signal.

To improve the control algorithm's ability to deal with high speed transient changes, an additional proportional control feedback was implemented in parallel to the IMC, adding preemptive HV changes. As shown in the control algorithm diagram in Fig. 1(a), the proportional feedback added to the IMC feedback value was calculated by multiplying the error between the current signal amplitude and the target signal amplitude with empirical coefficients determined experimentally. Since HV transient fall time is larger than the rise time, different coefficients were used depending on the sign of the error (ε). The proportional and IMC feedbacks were combined and sent to the HV power supply as a command that resulted in an MCP HV bias change determining the signal amplitude for the next ms-TRFS measurement.

#228925 - $15.00 USD Received 10 Dec 2014; revised 19 Feb 2015; accepted 20 Feb 2015; published 25 Feb 2015

To evaluate the performance of the ms-TRFS system using closed-loop control, abrupt changes in fluorescence intensity were simulated using a tissue phantom and distinct excitation-collection geometry (probe-to-target distance). The phantom consisted in five cuboid blocks of silicone gel (Wacker, SilGel 612) containing R6G dye. The R6G solution (200 µM in Ethanol) was mixed in the silicone gel at 1: 10 by volume. After the ethanol in the mixture was evaporated, the silicone gel was vulcanized and cut into 5 mm wide and 5, 7, 5, 3 and 5 mm height for the five blocks, respectively. To study the effect of sudden fluorescence intensity changes with phantom geometry, the hand held fiber-optic probe described above was mounted on a 1 µm resolution linear servo stage (MX80L, Parker, Cleveland, OH, USA) and scanned across the phantom from 8 mm distance above its bottom at 1, 3, 5 and 10 mm/s speed. Initially the closed-loop control was disabled for the 1 mm/s line scan while using 2200 V fixed MCP-PMT HV bias instead. The HV bias of 2200 V was chosen empirically to optimize the signal amplitude using a fixed HV bias when scanning the phantom. Then the closed-loop control was enabled to test its performance of maintaining the signal amplitude during line scans over the silicone gel phantom at 3, 5 and 10 mm/s speed.

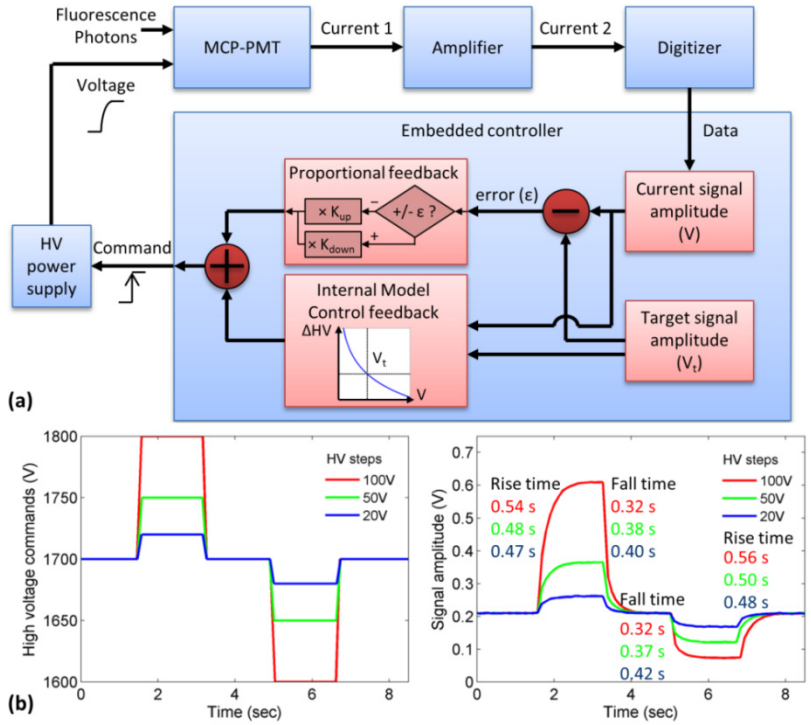

Fig. 1. (a) Closed-loop control diagram of ms-TRFS signal amplitude. After signal digitization the processor reads out the data and calculates feedback HV value using the control algorithm which consists of two controllers. The internal model controller (IMC) was based on the current gain characteristics of the MCP-PMT and the proportional controller was based on empirical linear coefficients multiplied to the error ε. (b) Transient response of the high voltage (HV) power supply. Left: Step-wise HV change commands sent to the power supply. Right: The ms-TRFS signal amplitude of a fluorescent dye recorded after receiving the commands. 10 – 90% rise time and 90 – 10% fall time of the transients are shown next to the edges.

2.3 ms-TRFS spatial resolution: Scanning mode with single fiber-optic

The spatial resolution of the scanning ms-TRFS system was defined as the full-width-half-maximum (FWHM) of the detected fluorescence intensity profile when the fiber is scanned across a sub-resolution target that is much smaller than the fiber core diameter. To determine

#228925 - $15.00 USD Received 10 Dec 2014; revised 19 Feb 2015; accepted 20 Feb 2015; published 25 Feb 2015

the spatial resolution for distinct probe-to-target distances an 80 µm fluorescent wire was used as the sub-resolution target and a liner scan (0.1 mm/s) was performed with the hand held fiber-optic probe positioned above the sample using the linear servo stage described above. The normalized fluorescence intensity of the ms-TRFS data, recorded continuously during the scanning, is shown in Fig. 2. The FWHM of the fluorescence intensity profile presented 288 µm, 287 µm, 322 µm and 565 µm spatial resolutions for 0, 1, 2 and 5 mm probe-to-target distance, respectively.

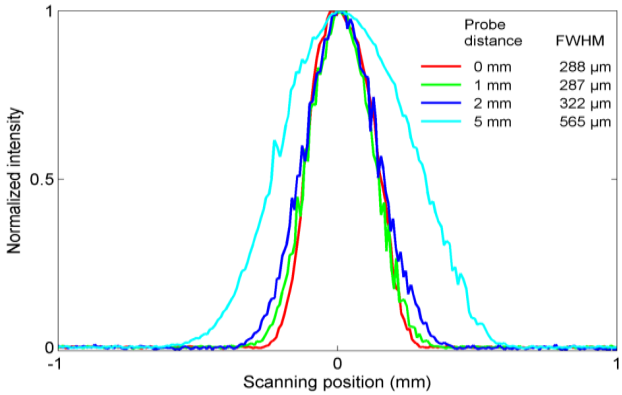

Fig. 2. Spatial resolution computed as the FWHM obtained by scanning across a sub-resolution target (80 µm fluorescent wire) at various distances using a 400 µm core 0.22 NA silica fiber integrated into a hand held probe.

2.4 Real-time ms-TRFS data processing and visualization

The fluorescence decay was recovered by deconvolving the instrument impulse response function (iIRF) from the measured fluorescence pulse transients. The iIRF characterizes the fluorescence pulse overall broadening due to optical dispersion and electronics [10]. For deconvolution we employed a fast algorithm (<1 ms per decay) previously reported by our group [12]. The algorithm is based on a constrained least-squares deconvolution with Laguerre expansion (CLSD-LE) method and has demonstrated robustness against noise. In this work, we adapted and implemented this algorithm in a portable package enabling integration with ms-TRFS system data acquisition software.

The practical implementation of the algorithm for continuous real-time processing of ms-TRFS data involves three distinctive steps. First, the iIRF pulse reference was aligned (on time-axis) with the measured data to provide correct deconvolution. Second, the aligned iIRF reference along with the Laguerre basis functions (which are the same regardless the characteristics of the measured signal) were computed and saved into memory buffer that can be accessed during on-line data processing. The final step involved calculating the solution of the non-negative least-squares (NNLS) problem in the CLSD-LE algorithm using the active set method [13] when a new ms-TRFS measurement was acquired. All steps were realized using OpenCV library [14] as an independent module for on-line data processing. In future developments, this can be further integrated with data classification and image processing modules. Currently the real-time data processing module was incorporated into the ms-TRFS system software platform using Labview (National Instrument) and implemented in the embedded controller of the system (Intel Celeron T3100, 1.90 GHz, 4 GB RAM, 32-bit Windows 7).

The performance of the data processing module in the integrated software (computation time and lifetimes standard deviation (SD)) was evaluated based on experimental measurements of Rhodamine 6G (200 µM in Ethanol). As previously demonstrated by simulation, the computation time and lifetimes SD are affected by the additive Gaussian noise

#228925 - $15.00 USD Received 10 Dec 2014; revised 19 Feb 2015; accepted 20 Feb 2015; published 25 Feb 2015

[12]. To evaluate the system's data processing performance two types of noises were evaluated: the Gaussian noise that was primarily introduced by the digitizer, and the Poisson noise that was introduced by the MCP-PMT. To separately evaluate the data processing performance under the influence of Gaussian and Poisson noise, R6G fluorescence was measured using the ms-TRFS system under various conditions. First, to study the data processing performance mainly affected by Gaussian noise, the signal amplitude and Gaussian noise root-mean-square [15] were varied for a fixed amount of optical signal. This was achieved by collecting fluorescence from R6G dye solution through the hand held fiber-optic probe described above at fixed distance (resulting in ~3.8×10^5 fluorescence photons at MCP-PMT) using different HV bias levels and averaging factors (number of laser pulses used to generate a fluorescence decay). Second, to study the data processing performance affected by Poisson noise, the number of detected photons was varied by changing fiber-to-sample distance, while the signal amplitude was maintained in a similar range (above 600 mV) with a constant averaging factor of 64. For each condition mentioned above, 1000 repeated measurements were taken, and the computation time was quantified as the average time of processing per fluorescence decay, while the lifetime SD was quantified as the standard deviation of the 1000 estimated lifetimes.

In current configuration, the integrated software platform provides real-time display of the raw ms-TRFS waveforms and visualization of processed data in three graphical formats (i.e. scaled lifetime plots, color coded graphs, and numeric values). The ms-TRFS waveforms can be used to assess the signal amplitude and the primary emission band of the fluorophore. The scaled lifetime plots provide lifetime values and color coded graphs provide direct visual contrast of lifetimes. A numeric lifetime value display was added to the axis origin of the color coded graph, showing dynamically the lifetime numerical values. Other fluorescence decay parameters, such as the Laguerre coefficients representing the dynamics of the fluorescence decay, are also available on-line and enable further data analysis if needed.

The overall performance of the integrated software, which includes data acquisition, data processing and visualization modules, was evaluated using program counter to quantify the execution time of all modules. Typical values of the software execution time were assessed using R6G dye solution measurements described above.

2.5 Tissue phantoms to evaluate ms-TRFS technical performance

To evaluate the performance of the ms-TRFS system for measuring various fluorophores with varying concentrations and on-line display of lifetime values experiments were conducted in two tissue phantoms as detailed below. Four fluorescence dyes were used in the experiments, i.e. Rodamine 6G (R6G), Coumarin 1 (C1), Coumarin 120 (C120) and 9-cyanoanthracene (9CA), which were all embedded in vulcanized silicone gel (Wacker, SilGel 612) as described above in section 2.2.

Phantom 1 was designed to study the system's ability to dynamically resolve distinct fluorophore species. For this, three fluorescence dyes, C1 (100 μM in Ethanol), C120 (250 μM in Ethanol) and 9CA (10 mM in Ethanol) were mixed in silicone gels (1:10 by volume) to fabricate three distinct phantom blocks with close fluorescence emission peaks (430 nm, 445 nm and 440 nm, respectively) but distinct lifetimes. Single-point static ms-TRFS measurements were recorded as reference of the fluorophores lifetimes in silicone gel. The corresponding lifetime values were 2.23 ± 0.03 ns, 2.70 ± 0.03 ns and 8.44 ± 0.01 ns in channel 1 and 2.75 ± 0.16 ns, 2.85 ± 0.11 ns and 8.32 ± 0.01 ns in channel 2.

Phantom 2 was designed to dynamically sense changes in fluorophores concentration. It consisted in R6G (200 μM in Ethanol) mixed in silicone gel at 1: 1, 1:10 and 1:100 by volume ratio, creating distinct concentrations of 200 μM, 20 μM and 2 μM, respectively. A silicone gel block was generated for each concentration. Single-point static ms-TRFS measurements of R6G mixed in silicone gel (20 μM) were recorded as reference with lifetime values of 3.33 ± 0.05 ns.

#228925 - $15.00 USD Received 10 Dec 2014; revised 19 Feb 2015; accepted 20 Feb 2015; published 25 Feb 2015

The silicone gels were aligned into rows for line scanning (0.5 mm/s) using the hand held fiber-optic probe described above, which was mounted on the linear servo stage at 1 mm distance from the top surface of the phantom. The length of the silicone gel blocks was measured along the scanning dimension, which were 5 mm for the C1, C120, 9CA blocks and 4.5, 4, 4.5 mm for 200 μM, 20 μM, 2 μM R6G blocks, respectively.

2.6 Tissue phantoms to demonstrate proof-of-concept for potential application

Two tissue phantoms were designed to mimic potential clinical applications of the scanning ms-TRFS system with real-time diagnostic feedback. One was designed to demonstrate the integration of the ms-TRFS system into a needle biopsy probe through a single fiber-optic and the ability of the system to resolve distinct tissue layers interface in real-time (mimic role in biopsy guidance). The other was designed to demonstrate the ms-TRFS ability to operate in conjunction with a hand held scanning fiber-optic probe and as a means to interrogate large tissue areas (e.g. surgical margins) and to identify otherwise undetectable lesion. Clinical situation mimicked in this study are similar with those encountered in clinical management of brain tumors.

2.6.1 Phantom and experiment for mimicking a needle biopsy application

Agar tissue phantom material (2% agar, 0.5% SiO_2 by weight in water) was casted into a brain mold to form the body of the phantom. Two one-inch diameter, 5 mm thick circular agar disks containing C1 and C120 dyes was embedded into the phantom approximately 15 mm under surface. The needle fiber-optic probe described above was mounted on a 45 μm resolution stepper motor stage (MX80S, Parker, Cleveland, OH, USA) and advanced into the phantom at 1 mm/s from 0 to 35 mm depth. Single point ms-TRFS measurements of the agar layers were recorded prior to the experiment and used as lifetime value reference. The null agar layer showed 2.55 ± 0.07 ns, 2.66 ± 0.04 ns and 3.63 ± 0.09 ns lifetimes for channel 1, 2 and 3. The C120 agar layer showed 4.52 ± 0.03 ns lifetime for channel 2. The C1 agar layer showed 1.71 ± 0.02 ns and 1.83 ± 0.08 ns lifetimes for channel 2 and 3.

To demonstrate potential applications, the real-time ms-TRFS results display was recorded in synchronization with a movie of the needle fiber-optic probe advancement into the phantom, which were merged into a single video (see Media 1 and Media 2 in section 3). The ms-TRFS waveform data was also recorded with time stamps, which were processed using standard post-processing software to generate reference lifetime values results. To avoid displaying unreliable results due to low signal-to-noise ratio (SNR), a 50 mV signal amplitude threshold was applied to the lifetime on-line display as well as post-processed results. (Same protocol was applied in the following sections).

2.6.2 Phantom and experiment for fluorescence marker identification by hand held raster scanning

A brain-shaped phantom body was built as describe in the previous section, then a cavity was created in the phantom body and filled with agar material containing a fluorescent dye: C120 (250 μM in Ethanol, 1:10 by volume). Thereafter, a 3 mm cubic silicone gel block (mixed with 0.5% SiO_2 by weight, and C1 100 μM in Ethanol, 1:10 by volume) was embedded in the area filled with C120-fluorescent agar to simulate a residual pathologically positive area.

To mimick examination of a surgical margin, the hand held fiber-optic probe described above was used to perform manual raster scanning on the phantom surface. The scanning was performed by an operator who has no prior knowledge of the location of fluorescence marker. The ms-TRFS system was displaying the lifetime of the interrogated area in real-time for the operator to identify the location of the fluorescence marker. Based on single point measurements, the lifetime in channel 2 (the channel in which the emission spectra of the marker and the fluorescent agar overlap) was 2.75 ns for the fluorescence marker and 4.51 ns

#228925 - $15.00 USD Received 10 Dec 2014; revised 19 Feb 2015; accepted 20 Feb 2015; published 25 Feb 2015

for the fluorescent agar. The experimental protocol described above was conducted to record both real-time results as well as original ms-TRFS waveform data for post-processing.

2.7 Biological tissue preparation and characterization

To demonstrate real-time fluorescence characterization of endogenous fluorophores with realistic quantum yields, a rat brain and its surrounding tissues were characterized *in situ* using the ms-TRFS system and the hand-held fiber-optic probe described above. A terminal rat from an unrelated study was used for this testing. Thirty minutes after the rat was sacrificed, it was mounted on a stereotactic frame (Kopf Small Animal Stereotaxic Frame Model 900, David Kopf Instruments, Tujunga, CA) and the brain was exposed through craniotomy surgery. The dura mater was removed to allow direct examination of the cerebral cortex. The hand held fiber-optic probe was mounted on the stereotactic frame to perform a coordinated manual line scan of 20 mm in approximately 20 seconds that the starting and ending locations were read precisely from the frame. The on-line ms-TRFS results as well as the ms-TRFS waveform data were recorded according to the aforementioned experimental protocol. Approximate location along the line scan can be estimated based on the time stamp of the measurement.

3. Results and discussion

3.1 Evaluation of fluorescence signal detection using closed-loop control

The ability of the ms-TRFS to accurately resolve the fluorescence lifetimes in real-time during sudden changes of probe-to-target distance is shown in Fig. 3. The signal amplitude of the line scan at 1 mm/s (no closed-loop control, fixed HV bias) reflects the actual variation in fluorescence intensity due to changes in phantom geometry. As expected, the intensity decreased as the probe-to-target distance increased. The baseline signal amplitude was 0.2 V at 3 mm distance and the maximum signal amplitude was 0.7 V at 1 mm distance. According to the current gain characteristics of the MCP, this indicates that the maximum signal amplitude would be exceeding the maximum range of the digitizer if the baseline amplitude was shifted to the targeted 0.3 V signal amplitude. The small changes in intensity for a constant distance were attributed to phantom inhomogeneity. The results for the 3 mm/s and 5 mm/s scan speeds (with closed-loop control) demonstrate that the signal amplitude was maintained within the dynamic range of the digitizer. For each step distance the signal amplitude returned to the target level of 300 mV before reaching the next step. For the 10 mm/s, the closed-loop controller was still effective in maintaining the signal amplitude within the digitizer dynamic range, although the signal amplitude did not reach the target level over 10 – 20 mm position. The signal amplitude briefly exceeded the maximum digitizer input voltage at the rising edge near 5 mm position.

The variation of the fluorescence lifetimes along the scanning positions (Fig. 3(c)) demonstrates good stability of lifetime measurement (3.31 ± 0.10 ns, 3.38 ± 0.08 ns, 3.38 ± 0.08 ns, and 3.32 ± 0.08 ns for 1, 3, 5 and 10 mm/s scan speeds, respectively). The boxplot of the overall statistic distribution of fluorescence lifetime values for each line scan ((Fig. 3(d)) show that the average lifetimes recovered for various scanning speeds with closed-loop control were consistent with the line scan with fixed HV bias.

These results show that the closed-loop control algorithm was capable of maintaining the signal amplitude within the dynamic range of the digitizer during dynamic excitation-collection geometry changes. In ms-TRFS practical application, the fluorescence quantum yield is unknown, finding an optimal fixed HV bias based on empirical adjustment during measurements can be unreliable and time-consuming. The use of closed-loop control enables rapid tissue evaluation without *a priori* information about its quantum efficiency.

#228925 - $15.00 USD Received 10 Dec 2014; revised 19 Feb 2015; accepted 20 Feb 2015; published 25 Feb 2015

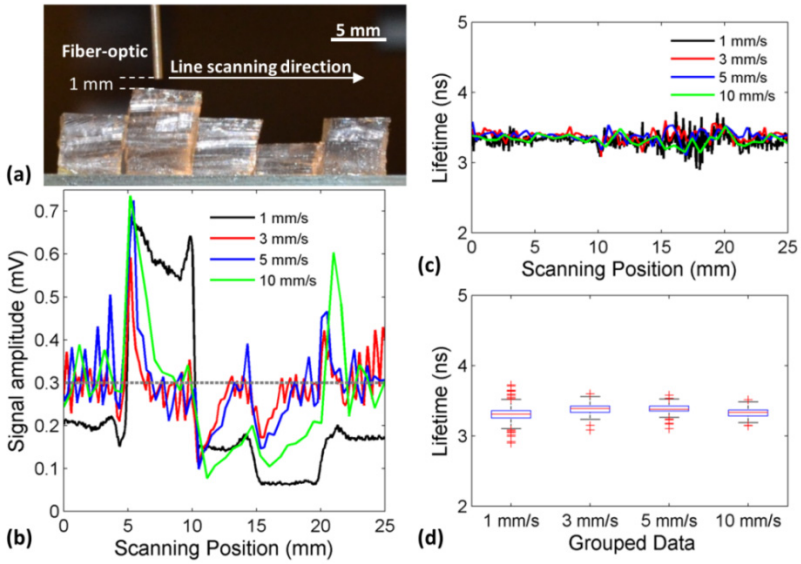

Fig. 3. Experiment for evaluation of close-loop control performance. (a) Close-up of the line-scanning setup. Picture of the 5 blocks (silicone gel mixed with R6G) with variable heights and the tip of the fiber optic probe. (b) Signal amplitude variation during the line scan. For reference the 1 mm/s line scan with fixed HV (closed-loop control disabled) was recorded. (c) Fluorescence lifetimes from each line scan (for channel 3). (d) Boxplot of the all lifetime values (line scans at different speeds). Box edges correspond to the 25 – 75% quartile and the whiskers correspond to the width extending 1.5 of the box width from each side of the box.

3.2 Evaluation of the real-time data processing

The performance (computation time and lifetime SD) of the data processing module was evaluated separately for the effect of Gaussian and Poisson noises. First, the effect of Gaussian noise on the real-time data processing was evaluated at 4 signal amplitude (30, 100, 280, and 680 mV) using 4 different averaging factors (1, 4, 16 and 64) with similar number of detected photons. The average computation time for a single fluorescence decay and its SD is shown in Fig. 4(a). Both decreased with higher signal amplitude and larger averaging factors, which indicates that better SNR enables faster and more robust data processing. This finding indicates that during dynamic time-resolved fluorescence measurement the closed-loop control can facilitate accurate and fast data processing by maintaining high signal amplitude. Data processing in 2.3 ± 0.05 ms per decay with < 0.04 ns lifetime SD can be reached at 280 mV signal amplitude using 64 averaging. Thus, the target signal amplitude of the closed-loop control was set at 300 mV and 64 averaging factor was adopted for the experiments in the following sections. As shown in Fig. 4(b), the lifetime SD also decreased with higher signal and lower noise (larger averaging factors), which agrees with previously reported simulation results [12].

Second, the effect of Poisson noise on the real-time data processing was evaluated using 5 different amounts of fluorescence photons, as shown in Fig. 4(c). The computation time and lifetime SD decreased as the number of photons increased. Since the Poisson noise is associated with the number of photons detected by the MCP-PMT, its effect cannot be compensated by the closed-loop control. The Poisson noise is the main source of error with 3.7×10^5 fluorescence photons and below. This poses an inherent limit to the system. Fortunately, most biological endogenous fluorophores provides enough fluorescence photons with the laser pulses used by the system, while complying with the ANSI UV exposure limit [16].

#228925 - $15.00 USD Received 10 Dec 2014; revised 19 Feb 2015; accepted 20 Feb 2015; published 25 Feb 2015

The overall performance of the integrated software was evaluated based on the execution time of the software during real-time measurements. Typical execution time for different modules of the software was quantified as following: the data acquisition and readout took 10 ms; the communication of querying and setting HV took 20 ms; the data processing to reconstruct the fluorescence decays in all ms-TRFS channels and calculate lifetime used 35 ms; and the rendering of ms-TRFS waveform and lifetimes typically used 10 ms. In total, each iteration of acquisition, processing and display of ms-TRFS data during the real-time process typically require 65 ms to execute and thus provide a continuous sampling rate of 15 Hz. Depending on the SNR and number of channels activated by the sample fluorescence, the sampling rate can vary from 10 to 20 Hz, which is still suitable for most tissue characterization application of the technique. In order to improve the speed of the system, future design should adopt a HV power supply with better time response performance and a controller with higher computation power for faster data processing. Technically the speed of the system could reach the limit of the laser repetition rate and the speed of the digitizer, which is in the order of 100 kHz.

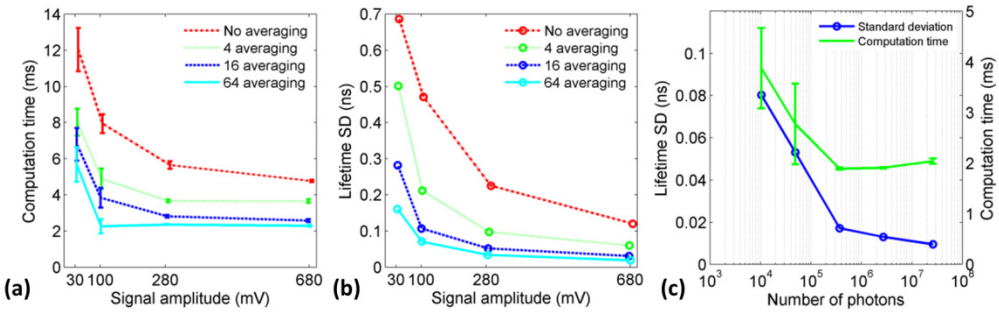

Fig. 4. (a) The single fluorescence decay computation time and (b) lifetime standard deviation (SD) were quantified with various signal amplitude and averaging factors using same number of photons detected (3.8×10^5 photons). (c) The single fluorescence decay computation time and lifetime standard deviation were quantified using different number of photons.

3.3 ms-TRFS technical performance

The ability of ms-TRFS to dynamically resolve distinct fluorophore species and changes in fluorophore concentration is depicted in Fig. 5.

The three fluorophores in Phantom 1 (C1, C120 and 9CA) were differentiated by the system based on lifetimes, despite of their similar emission spectra. In Fig. 5(e), the lifetime of the fluorophores of each block, presented lifetime values of 2.25 ± 0.04 ns, 2.71 ± 0.03 ns, 8.42 ± 0.01 ns in channel 1 and 2.81 ± 0.20 ns, 2.84 ± 0.12 ns, 8.33 ± 0.06 ns in channel 2 for C1, C120 and 9CA, respectively. Similar relative ratio of fluorescence photons between channel 1 and 2 was observed for the three fluorophores, as shown in Fig. 5(c). The results agreed very well with the single point ms-TRFS measurements recorded prior to the line scan.

The fluorophore concentration variation in Phantom 2 was detected by the number of collected fluorescence photons quantified based on the ms-TRFS measurements (Fig. 5(d)), while similar lifetimes were retrieved from the same fluorophore in different concentrations (Fig. 5(f)). The resulting fluorescence lifetimes values were 3.45 ± 0.03 ns, 3.28 ± 0.05 ns and 3.25 ± 0.07 ns for 200 μM, 20 μM and 2 μM concentrations, respectively. For the two low concentrations, the results were consistent with the static single point measurement prior to the line scan. Small variation (~0.2 ns) was observed between the silicone gels with high and low R6G concentrations. This can be explained by the formation of dye molecule dimers with high concentration versus only monomers for low concentration, which present slightly different lifetimes [17].

#228925 - $15.00 USD Received 10 Dec 2014; revised 19 Feb 2015; accepted 20 Feb 2015; published 25 Feb 2015

These experiments demonstrate that ms-TRFS system provides accurate differentiation of distinct fluorophores species and robust lifetime measurement regardless of fluorophore concentration during scanning.

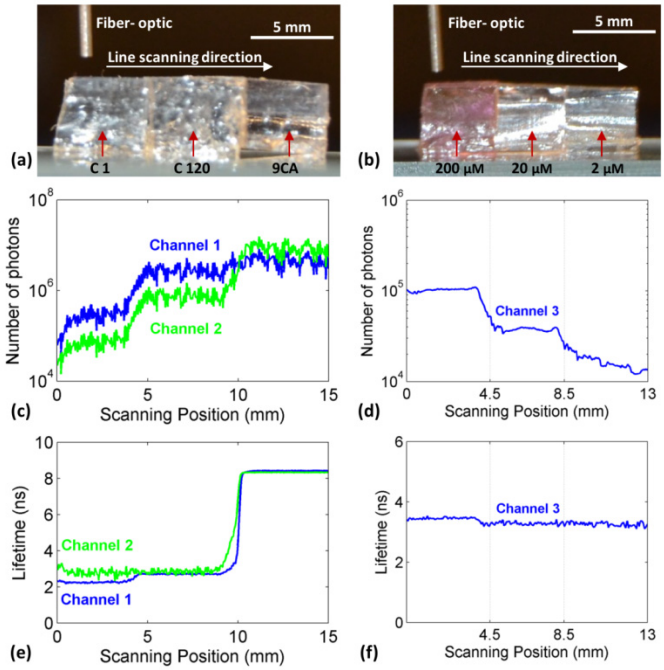

Fig. 5. Real-time ms-TRFS line scanning measurement of fluorescence phantoms with fluorophore species and concentration changes. (a – b) Close-up of Phantom1 with three distinctive species of fluorophores (C1, C120 and 9CA) and Phantom 2 with three different fluorophore concentrations (200 µM, 20 µM, 2µM). (c – d) The number of fluorescence photons collected during the line scan quantified based on the fluorescence intensity. (e – f) The fluorescence lifetime profile of the line scans.

3.4 Proof-of-concept: needle biopsy application

The potential application of the ms-TRFS in conjunction with needle biopsy is demonstrated in Fig. 6. Two distinctive fluorescence layers were differentiated from the null agar material based on fluorescence lifetimes. The tissue phantom agar material provides fluorescence showing 2.56 ± 0.07 ns, 2.62 ± 0.05 ns and 3.66 ± 0.08 ns lifetime for channel 1, 2 and 3 for the top layer of the phantom (0 – 2 mm). Similar lifetime of the agar was observed at the bottom layer of the phantom (30 – 35 mm), presenting 2.52 ± 0.08 ns, 2.64 ± 0.09 ns and 3.61 ± 0.09 ns for channel 1, 2, and 3. The C120 layer presented 4.51 ± 0.02 ns lifetime in channel 2 at scanning position from 14 – 20 mm. The C1 layer presented 1.74 ± 0.02 ns in channel 2 and 1.88 ± 0.08 ns in channel 3 at scanning position from 24.5 – 25.5 mm.

The on-line lifetime display of the ms-TRFS software is demonstrated in Fig. 6(c) and in Media 1. The top panel of the software shows the ms-TRFS waveform data and the bottom panel shows the scaled lifetime plots. The color coded graph of the lifetimes is shown in the middle panel with the numeric lifetime value of the current measurement shown on the left. As the probe is advanced into the phantom, the fluorescence lifetimes of different phantom layers are displayed in real-time and were found consistent with the post-processed results.

These results demonstrate the concept of performing real-time tissue characterization using the ms-TRFS during needle biopsy by the detection of different layers in the fluorescence phantom. In current phantom, the boundaries of the layers could not be preserved because the fluorophores were migrating among the agar layers once put in contact.

#228925 - $15.00 USD Received 10 Dec 2014; revised 19 Feb 2015; accepted 20 Feb 2015; published 25 Feb 2015

This will not be the case for biological tissues, so delineation of distinct tissue layers can potentially be achieve with accuracy close to the spatial resolution of the fiber-optics. Current single fiber-optic probe (480 μm total diameter) can be integrated into surgical needle biopsy tools to enable simultaneous characterization of local tissue fluorescence and tissue ablation for needle biopsy.

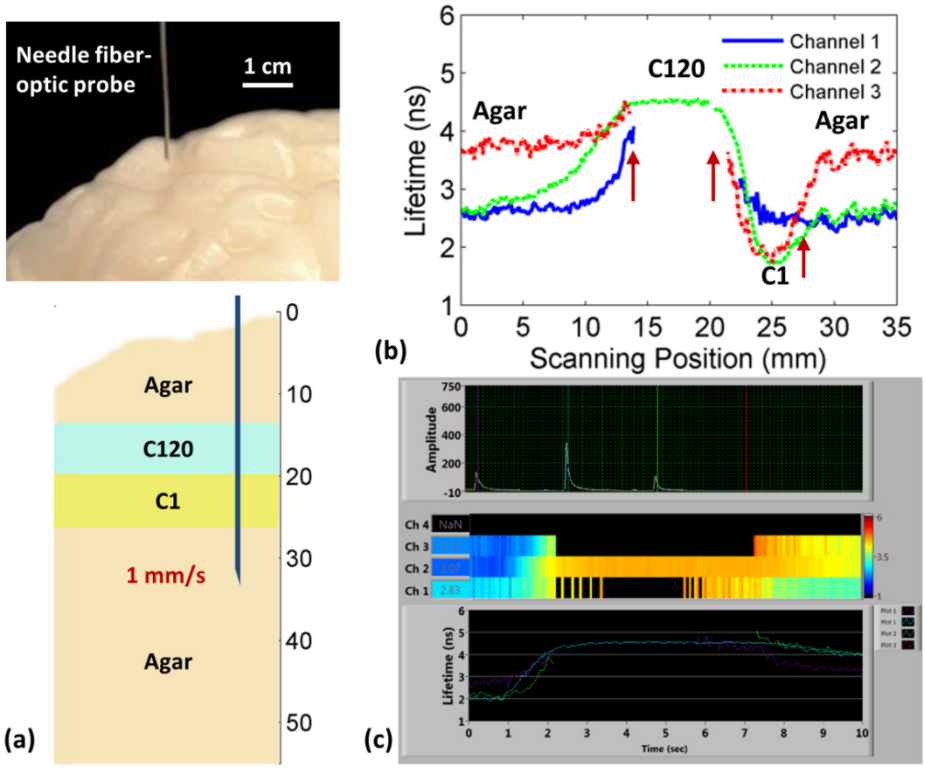

Fig. 6. Needle fiber-optic probe biopsy of a brain shaped phantom embedded with two fluorescent agar layers. (a) Top: A picture of the needle fiber-optic probe advancing into the phantom; Bottom: Schematic of the layered phantom and biopsy setup. The needle fiber-optic probe was advanced by a motorized stage to penetrate through different layers of the phantom at 1 mm/s speed. The interfaces between null agar – C120 agar, C120 agar – C1 agar and C1 agar – null agar were located at approximately 14, 20 and 27 mm depth in the phantom. (b) Post-processed fluorescence lifetime profile during the biopsy. Red arrows show the interfaces between layers. (c) Screen shot of ms-TRFS software displaying the results in real-time. (See Media 1 for a video of the experiment.)

3.5 Proof-of-concept: fluorescence marker identification

The potential application of ms-TRFS as means to evaluate the surgical resection margins is demonstrated in Fig. 7. The fluorescence marker was successfully identified by the operator based on fluorescence lifetime, despite that the marker was not visually differentiable from the background fluorescent agar under white light and UV illumination. The fluorescence marker was identified by decreased lifetime values during the raster scanning as indicated by the red arrows (3.27 ns, 3.13 ns, 3.12 ns and 3.02 ns). As shown in Media 2, detection of the fluorescence marker was signaled by the drop of lifetime in the scaled lifetime plot as well as the change of color in the color coded graph when the hand held fiber-optic probe scanned across the area indicated by the red arrow (the marker).

The change of fluorescence intensity during the free hand held raster scanning is shown in Fig. 7(c) by the fluorescence photons variations. The closed-loop control of the ms-TRFS system were able to maintain effective fluorescence detection that resulted in continuous

#228925 - $15.00 USD Received 10 Dec 2014; revised 19 Feb 2015; accepted 20 Feb 2015; published 25 Feb 2015

display of fluorescence lifetime and consistent lifetime values (4.51 ± 0.04 ns) of the C120 fluorescent agar regardless of the fluorescence intensity variation.

Partial volume effect was observed because the beam size was comparable to the size of the marker. The lifetime values extracted at the red arrowed area were a weighted average between the lifetimes of the fluorescence marker (2.75 ns) and the C120 fluorescent agar (4.51 ns). Since the beam size is a function of probe to sample distance, in practical application this can be addressed by reducing the distance to achieve better spatial resolution.

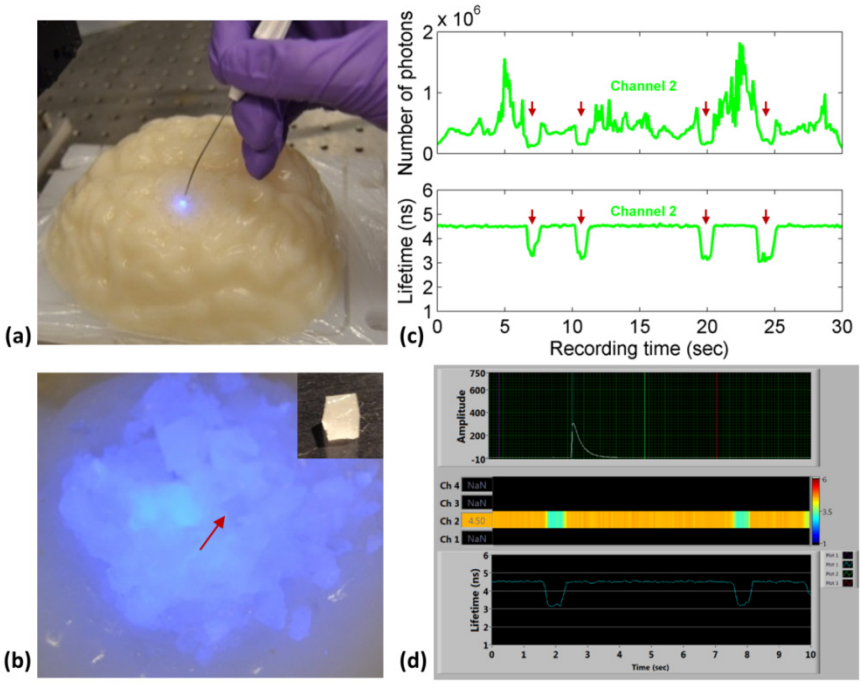

Fig. 7. Identification of fluorescence marker by surface scanning of hand held probe in a brain shaped agar phantom. An excision cavity were created and filled with agar mixed with fluorescent dye (C120). A fluorescent silicone gel block (C1) was embedded in the cavity as a distinct fluorescence marker. (a) A picture of raster scanning using the hand held fiber-optic probe on the surface of the cavity. (b) A fluorescent intensity image of the cavity taken under wide-field UV illumination. The location of the embedded marker is shown by the red arrow. A close-up of the fluorescence marker is shown at top right. (c) The number of fluorescence photons and fluorescence lifetime profile during the hand held scanning. The red arrows show the identification of the marker. (d) A screen shot of the real-time display during the test. (See Media 2 for a complete video of the experiment)

The concept of using the ms-TRFS system to characterize large tissue area intra-operatively was demonstrated in this test. Current system using hand held fiber-optic probe can provide a fast, flexible and non-invasive means of assessing tissue chemical characteristics for future intra-operative guidance.

3.6 Real-time tissue characterization

The application of the ms-TRFS system on biological tissue with realistic quantum yield is demonstrated in Fig. 8. Distinctive tissue types were identified and differentiated under *in situ* condition. The brain cortex areas presented lifetimes of 3.13 ± 0.17 ns, 2.27 ± 0.07 ns, 1.95 ± 0.16 ns in channel 1, 2, 3, respectively. The exposed bone tissue of skull and the vessel in superior sagittal sinus were distinguished from the brain matter by the longer lifetime values in all three channels. The thin muscle tissue surrounding the skull presented distinctive fluorescence lifetimes of 3.15 ± 0.20 ns, 1.86 ± 0.18 ns, and 1.58 ± 0.18 ns in channel 1, 2 and

#228925 - $15.00 USD Received 10 Dec 2014; revised 19 Feb 2015; accepted 20 Feb 2015; published 25 Feb 2015

3, respectively. The fluorescence of major endogenous fluorophores was captured by different channels of the ms-TRFS system. Channel 1 is mainly associated with the collagen and elastin fluorescence, channel 2 is mainly associated with NADH and elastin fluorescence and channel 3 is associated with FAD fluorescence. The differences of lifetimes between channels for the same type of tissue are related to the differences of spectral contributions to the ms-TRFS channels for various endogenous fluorophores.

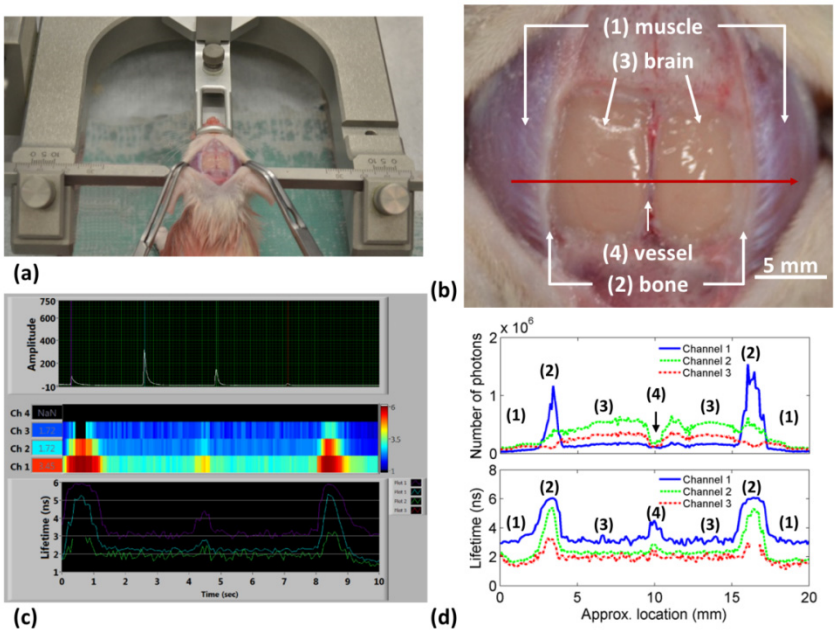

Fig. 8. Characterization of biological tissue by real-time ms-TRFS. (a) A picture of the stereotactic frame setup mounted on the sacrificed rat. (b) A close-up of the expose brain cortex of the rat with different tissue types denoted along the line scan (red arrow). (1) the muscle tissue covering the skull; (2) exposed bone tissue after craniotomy surgery; (3) exposed brain matter after removal of dura matter; (4) Blood vessel in superior sagittal sinus; (c) A screen shot of real-time display during the line scan. (d) Top panel: number of collected fluorescence photons along the line scan; bottom panel: fluorescence lifetimes along the line scan. The approximate location along the line scan was estimated based on the scanned length and total scanning time. The differentiated tissue types were denoted according to (b).

The robustness of the ms-TRFS system using closed-loop control was tested by the complex excitation-collection geometry changes and fluorophore quantum yield variations of the sample. The brain cortex areas showed fluorescence intensity variation mainly due to changes in probe-to-target distance, while the measured fluorescence lifetimes values remained consistent. The blood vessel showed much less fluorescence intensity compared to bone and brain matter due to blood absorption, while the change in lifetime was still detected under this situation.

This application of the ms-TRFS system in practical setup using in situ biological tissue showed the system's ability to reliably analyze distinct types of tissue with various fluorescence quantum efficiencies.

4. Conclusion

Current study demonstrates a scanning multispectral time-resolved fluorescence spectroscopy technique with self-adjustable photon detection range through a novel closed-loop control algorithm. This technique enables robust continuous acquisition and real-time display (<100 ms) of fluorescence decay parameters regardless of dynamic changes in fluorescence

#228925 - $15.00 USD Received 10 Dec 2014; revised 19 Feb 2015; accepted 20 Feb 2015; published 25 Feb 2015

excitation-collection geometry or sample fluorescence quantum yield. Data acquisition, processing and display were implemented in an efficient and integrated software package. Overall, the integrated system software enabled rapid acquisition of fluorescence decay data in multiple spectral bands and on-line display of the computed decay parameters (e.g. lifetime values) at 10 – 20 Hz. The robustness of the control algorithm was demonstrated in fluorescence phantoms using fiber-optic probes and realistic scanning parameters. Results from fluorescence phantoms demonstrated the ability of the system to dynamically resolve distinct fluorescent dyes. Two potential applications, needle biopsy guidance and surgical cavity examination were demonstrated in tissue phantoms and real-time biological tissue characterization was shown in a rat head with a craniotomy. Current results demonstrate that distinct biological tissues can be resolved in one continuous rapid scan regardless of the significant and dynamic changes in the total number of photons reaching the detector. Current findings demonstrate that ms-TRFS technique with self-adjustable photon detection can be integrated with current standard surgical procedure and show great potential as a tool for real-time tissue diagnosis intra-operatively.

Acknowledgments

This work was supported by the NIH R21 CA178578 and UCOP Grant No 13-PC-268121. The authors would like to thank Wacker Chemie for providing the SilGel product, Brad Hartl and Hussain Fatakdawala for their technical support during the experiments.

#228925 - $15.00 USD Received 10 Dec 2014; revised 19 Feb 2015; accepted 20 Feb 2015; published 25 Feb 2015